Journal of Thermal Analysis and Calorimetry (2018) 134:2295–2303
https://doi.org/10.1007/s10973-018-7866-7

CrossMark

Nanofluid heat transfer and entropy generation through a heat exchanger considering a new turbulator and CuO nanoparticles

M. Sheikholeslami[1,2] · M. Jafaryar[2,3] · Ahmad Shafee[4,5] · Zhixiong Li[6,7]

Received: 8 August 2018 / Accepted: 20 October 2018 / Published online: 31 October 2018

Abstract

In this research, a numerical macroscopic approach has been employed to analyze nanofluid entropy generation and turbulent flow through a circular heat exchanger with an innovative swirl flow device. A homogenous model was considered for nanofluid. Minimizing entropy generation can be considered as a very important goal for designing a heat exchanger, so we focus on this factor in the present attempt. Simulations were presented to show the influences of the geometric parameter (revolution angle) and inlet velocity on hydrothermal and second-law treatment. Related correlations for thermal and frictional entropy parameters as well as Bejan number have been presented. Outputs reveal that augmenting revolution angle increases the frictional entropy generation. Increasing secondary flows leads to a reduction in thermal entropy generation due to a decrement in thermal boundary layer thickness. By improving convective flow, Bejan number reduces.

Keywords Nanofluid · Heat transfer · Passive technique · Heat exchanger · Entropy generation

List of symbols

$S_{gen,f}$	Viscous entropy generation
Nu	Nusselt number
T	Fluid temperature
Re	Reynolds number
P	Pressure
L	Length of pipe
f	Darcy friction factor
Pr	Prandtl number
$S_{gen,th}$	Thermal entropy generation
D	Pipe diameter

Greek symbols

α	Thermal diffusivity
ϕ	Concentration of nanofluid
μ	Dynamic viscosity of nanofluid
ρ	Density
β	Revolution angle

Subscripts

s	Particles
nf	Working fluid
f	Fluid

Introduction

To reach the best design of a heat exchanger, both hydrothermal and second-law behaviors need to be considered. To enhance its efficiency, nanofluid can be considered as a working fluid in a heat exchanger. Nanofluids have many applications, such as in solar energy [1], solidification/melting

✉ Zhixiong Li
zhixiongli.cumt@gmail.com

1 Department of Mechanical Engineering, Babol Noshirvani University of Technology, Babol, Islamic Republic of Iran

2 Renewable Energy Systems and Nanofluid Applications in Heat Transfer Laboratory, Babol Noshirvani University of Technology, Babol, Iran

3 MR CFD LLC, No 49, Gakhokidze Street, Isani-Samgori District, Tbilisi, Georgia

4 FAST, University Tun Hussein Onn Malaysia, 86400 Parit Raja, Batu Pahat, Johor State, Malaysia

5 Applied Science Department, College of Technological Studies, Public Authority of Applied Education and Training, Shuwaikh, Kuwait

6 School of Engineering, Ocean University of China, Qingdao 266110, China

7 School of Mechanical, Materials, Mechatronic and Biomedical Engineering, University of Wollongong, Wollongong, NSW 2522, Australia

enhancement [2, 3], condensation process [4]. Jafaryar et al. [5] suggested the innovative twisted tape with an alternate axis to generate secondary flows in a heat exchanger. They utilized nanofluid as an effective fluid. Jafaryar et al. [6] displayed turbulent migration of nanofluid through a pipe. They used two combined passive techniques to reach the best design. Haq et al. [7] depicted the MHD mixed convection over a sheet. Qi et al. [8] reported experimental results for nanofluid heat transfer augmentation in a heat exchanger. They analyzed the stability of working fluid. Sheikholeslami et al. [9] demonstrated exergy loss of nanofluid in a pipe with a swirling device. They presented correlations for destroyed exergy. Zheng et al. [10] demonstrated sensitivity analysis for a flat heat exchanger to find the impact of active parameters on the thermal behavior. Sajjadi and Kefayati [11] studied the turbulent-free convection in an enclosure. They used a mesoscopic approach in their attempt. Zheng et al. [12] utilized vortex rods for augmentation of efficiency of the heat exchanger. They simulated the current problem for laminar region. Astanina et al. [13] demonstrated the second- and first-law approach for ferrofluid natural convection within a cavity. They simulated the nanofluid behavior under the role of Lorentz forces. Choosing a good working fluid is the hot subject in recent decades [14–43].

Although the hydrothermal behavior of nanofluid laminar flow within a heat exchanger has been reported by previous researchers, there are few papers in which researchers focus on entropy generation of nanofluid. Also, in the current paper, we present an innovative type of turbulator to enhance the efficiency. For better estimation of the behavior of working fluid, previous experimental models have been utilized. Impact of inlet velocity and revolution angle on nanofluid flow, frictional and thermal entropy generations is shown as contours.

Physical model

Two passive techniques have been employed in the current study. Using nanofluid and a turbulator can improve the heat transfer. Properties of H_2O and CuO nanoparticles were depicted in Tables 1 and 2. Single phase was utilized for working fluid by employing experimental correlations. A new shape of the turbulator has been selected (see Fig. 1). Revolution angle was considered as a geometric variable. Length of the pipe is 900 mm, and the test section is central 300 mm. The reason for selecting such test section is because of the fact that test section should not appear any back flow. The inlet boundary was considered as velocity inlet and the outlet one was pressure outlet. The heat exchanger is heated by a constant heat flux.

Table 1 Coefficients of CuO–water

Coefficient values	CuO–water
a1	−26.5933108
a2	−0.403818333
a3	−33.3516805
a4	−1.915825591
a5	6.421858E − 02
a6	48.40336955
a7	−9.787756683
a8	190.245610009
a9	10.9285386565
a10	−0.72009983664

Table 2 Properties of base fluid and nanoparticles

	ρ/kg m^{-3}	C/j kgk^{-1}	k/W m.k^{-1}	μ/Pa.s
Pure water	997.1	4179	0.613	0.0010003
CuO	6500	540	18	–

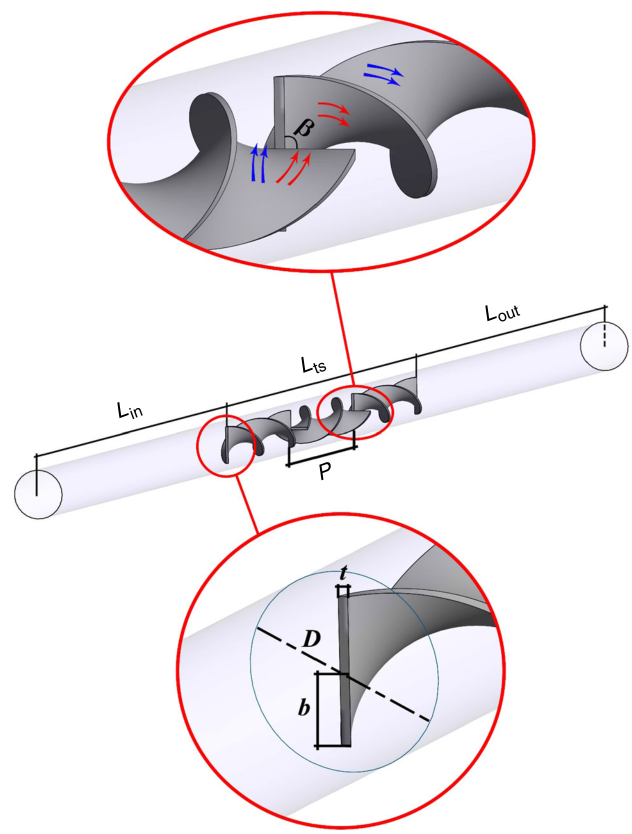

Fig. 1 Present heat exchanger

Problem formulation

A heat exchanger with a turbulator is simulated in the current attempt. Turbulent nanofluid flow is considered. Governing partial equations for such flow are:

$$\frac{\partial(u_{\mathrm{i}})}{\partial x_{\mathrm{i}}}=0 \tag{1}$$

$$\frac{\partial}{\partial x_{\mathrm{j}}}\left(\rho_{\mathrm{nf}}u_{\mathrm{i}}u_{\mathrm{j}}\right)=-\frac{\partial p}{\partial x_{\mathrm{i}}}+\frac{\partial}{\partial x_{\mathrm{j}}}\left(\left(\frac{\partial u_{\mathrm{i}}}{\partial x_{\mathrm{j}}}+\frac{\partial u_{\mathrm{j}}}{\partial x_{\mathrm{i}}}\right)\mu_{\mathrm{nf}}\right)+\frac{\partial}{\partial x_{\mathrm{j}}}\left(-\rho_{\mathrm{nf}}\overline{u_{\mathrm{j}}'u_{\mathrm{i}}'}\right) \tag{2}$$

$$\frac{\partial}{\partial x_{\mathrm{i}}}\left(\rho_{\mathrm{nf}}Tu_{\mathrm{i}}\right)=\frac{\partial}{\partial x_{\mathrm{i}}}\left((\Gamma_{\mathrm{t}}+\Gamma)\frac{\partial T}{\partial x_{\mathrm{i}}}\right),\quad \Gamma_{\mathrm{t}}=(\mu_{\mathrm{t}}/Pr_{\mathrm{t}}),\quad \Gamma=(\mu_{\mathrm{nf}}/Pr_{\mathrm{nf}}), \tag{3}$$

$\rho_{\mathrm{nf}}\overline{u_{\mathrm{j}}'u_{\mathrm{i}}'}$

and μ_{t} are:

$$-\rho_{\mathrm{nf}}\overline{u_{\mathrm{i}}'u_{\mathrm{j}}'}=\left(\frac{\partial u_{\mathrm{i}}}{\partial x_{\mathrm{j}}}+\frac{\partial u_{\mathrm{j}}}{\partial x_{\mathrm{i}}}\right)\mu_{\mathrm{t}}-\frac{2}{3}\rho_{\mathrm{nf}}k\delta_{\mathrm{ij}}-\frac{2}{3}\mu_{\mathrm{t}}\frac{\partial u_{\mathrm{k}}}{\partial x_{\mathrm{k}}}\delta_{\mathrm{ij}} \tag{4}$$

$$\mu_{\mathrm{t}}=\frac{1}{\varepsilon}k^2C_{\mu}\rho_{\mathrm{nf}} \tag{5}$$

Due to strong swirling flow, we selected $k-\varepsilon$ model and checked the limitation of this model. A homogenous model is employed for estimating nanofluid properties:

$$\frac{\partial}{\partial x_{\mathrm{j}}}\left((\mu_{\mathrm{nf}}+\mu_{\mathrm{t}}/\sigma_{\mathrm{k}})\frac{\partial k}{\partial x_{\mathrm{j}}}\right)+G_{\mathrm{k}}-\rho_{\mathrm{nf}}\varepsilon=\frac{\partial}{\partial x_{\mathrm{i}}}(u_{\mathrm{i}}k\rho_{\mathrm{nf}}),\quad G_{\mathrm{k}}=-\rho_{\mathrm{nf}}\frac{\partial u_{\mathrm{j}}}{\partial x_{\mathrm{i}}}\overline{u_{\mathrm{j}}'u_{\mathrm{i}}'} \tag{6}$$

$$\frac{\partial}{\partial x_{\mathrm{i}}}(u_{\mathrm{i}}\rho_{\mathrm{nf}}\varepsilon)=\frac{\varepsilon}{k}G_{\mathrm{k}}C_{1\varepsilon}-\rho_{\mathrm{nf}}\frac{\varepsilon^2}{k}C_{2\varepsilon}+\frac{\partial}{\partial x_{\mathrm{j}}}\left(\left(\frac{\mu_{\mathrm{t}}}{\sigma_{\varepsilon}}+\mu_{\mathrm{nf}}\right)\frac{\partial\varepsilon}{\partial x_{\mathrm{j}}}\right) \tag{7}$$

$$C_{1\varepsilon}=1.42,\quad C_{\mu}=0.0845,\quad C_{2\varepsilon}=1.68,\quad Pr_{\mathrm{t}}=0.85,\quad \sigma_{\mathrm{k}}=1,\quad \sigma_{\varepsilon}=1.3 \tag{8}$$

ANSYS Fluent has been used for simulation. Pressure-based solver has also been used. We simulate a steady-state form. SIMPLE algorithm was selected for coupling of pressure and velocity. Upwind method was employed for discretization.

ρ_{nf}, $(\rho C_p)_{\mathrm{nf}}$, μ_{nf} and $k_{\mathrm{nf}}\mu_{\mathrm{nf}}$ are [44]:

$$\rho_{\mathrm{nf}}=\rho_{\mathrm{f}}(1-\phi)+\rho_{\mathrm{s}}\phi \tag{9}$$

$$(\rho C_{\mathrm{p}})_{\mathrm{nf}}=-(\phi-1)(\rho C_{\mathrm{p}})_{\mathrm{f}}+(\rho C_{\mathrm{p}})_{\mathrm{s}}\phi \tag{10}$$

$$\frac{\mu_{\mathrm{nf}}}{\mu_{\mathrm{f}}}=[Prk_{\mathrm{f}}]^{-1}k_{\mathrm{Brownian}}+(1-\phi)^{-2.5} \tag{11}$$

$$\begin{aligned}\frac{k_{\mathrm{nf}}}{k_{\mathrm{f}}}&=1+3\frac{\phi(kk-1)}{-\phi(kk-1)+(2+kk)}+5\times10^4\phi\rho_{\mathrm{f}}c_{\mathrm{p,f}}\sqrt{\frac{\kappa_{\mathrm{b}}T}{\rho_{\mathrm{p}}d_{\mathrm{p}}}}g'(\phi,d_{\mathrm{p}},T)\\ g'(\phi,d_{\mathrm{p}},T)&=\Big(a_2Ln(d_{\mathrm{p}})+a_1+a_5Ln(d_{\mathrm{p}})^2+a_4Ln(d_{\mathrm{p}})Ln(\phi)+a_3Ln(\phi)\Big)Ln(T)\\ &\quad+\Big(a_{10}Ln(d_{\mathrm{p}})^2+a_6+a_8Ln(\phi)+a_7Ln(d_{\mathrm{p}})+a_9Ln(d_{\mathrm{p}})Ln(\phi)\Big),\\ kk&=k_{\mathrm{p}}/k_{\mathrm{f}}\end{aligned} \tag{12}$$

z = 0 and z = L have the following conditions:

$$v_{\mathrm{i}}=0,\quad w_{\mathrm{i}}=cte,\quad u_{\mathrm{i}}=0,\quad I=0.16(Re)^{\frac{-1}{8}},\quad T_{\mathrm{i}}=cte \tag{13}$$

$$\frac{\partial u}{\partial z}=\frac{\partial v}{\partial z}=\frac{\partial T}{\partial z}=\frac{\partial w}{\partial z}=0, \tag{14}$$

In the current work, the definitions of Nu and f are:

$$Nu=\frac{hD_{\mathrm{h}}}{k_{\mathrm{nf}}} \tag{15}$$

$$f=\frac{\Delta p}{\frac{\rho v_{\mathrm{m}}^2}{2}\frac{L}{D_{\mathrm{h}}}} \tag{16}$$

$S_{\mathrm{gen,th}}$ and $S_{\mathrm{gen,f}}$ were calculated as:

$$S_{\mathrm{gen,th}}=\frac{k_{\mathrm{nf}}}{T^2}\left[\left(\frac{\partial T}{\partial z}\right)^2+\left(\frac{\partial T}{\partial y}\right)^2+\left(\frac{\partial T}{\partial x}\right)^2\right], \tag{17}$$

Table 3 Example of mesh independency for $\beta=90°,\quad Re=20000$

Number of nodes	Nu
320,782	253.8415
371,067	258.7461
405,753	260.0394
464,125	260.5273

Table 4 Ranges of Y^+ for outer wall at Re = 20,000

β	Y^+
0°	4.5433044
45°	4.7648616
90°	4.79353

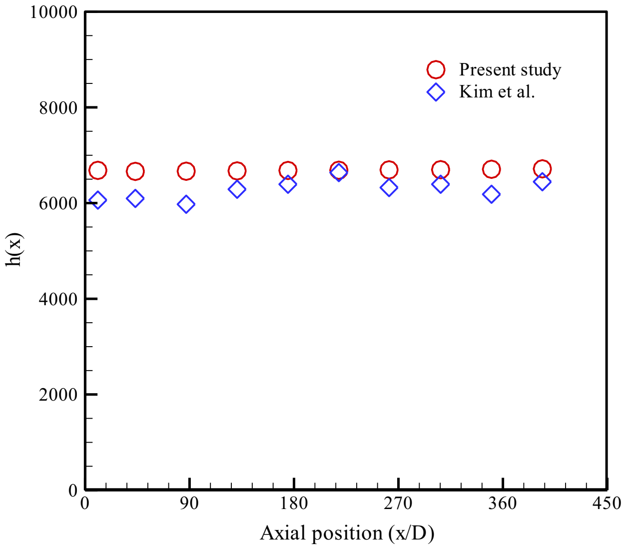

Fig. 2 Verification of our approach for *h(x)* [45]

$$S_{\mathrm{gen,f}} = \frac{\mu_{\mathrm{nf}}}{T}\left\{ \begin{array}{r} \left(\frac{\partial v}{\partial x}+\frac{\partial u}{\partial y}\right)^2 + 2\left[\left(\frac{\partial u}{\partial x}\right)^2+\left(\frac{\partial w}{\partial z}\right)^2+\left(\frac{\partial v}{\partial y}\right)^2\right] \\ +\left(\frac{\partial v}{\partial z}+\frac{\partial w}{\partial y}\right)^2+\left(\frac{\partial u}{\partial z}+\frac{\partial w}{\partial x}\right)^2 \end{array} \right\} \quad (18)$$

Each numerical simulation should have outputs without dependence on mesh. For the current attempt, grid independency analysis has been checked, and we presented an example in Table 3. Also, to satisfy the condition of the chosen turbulent model, Y^+ should be lower than 5. We checked this fact, which is presented in Table 4. For verification of the current code, a comparison with a previous article is depicted in Fig. 2 [45]. This figure proves great accuracy of the current code for nanofluid turbulent flow.

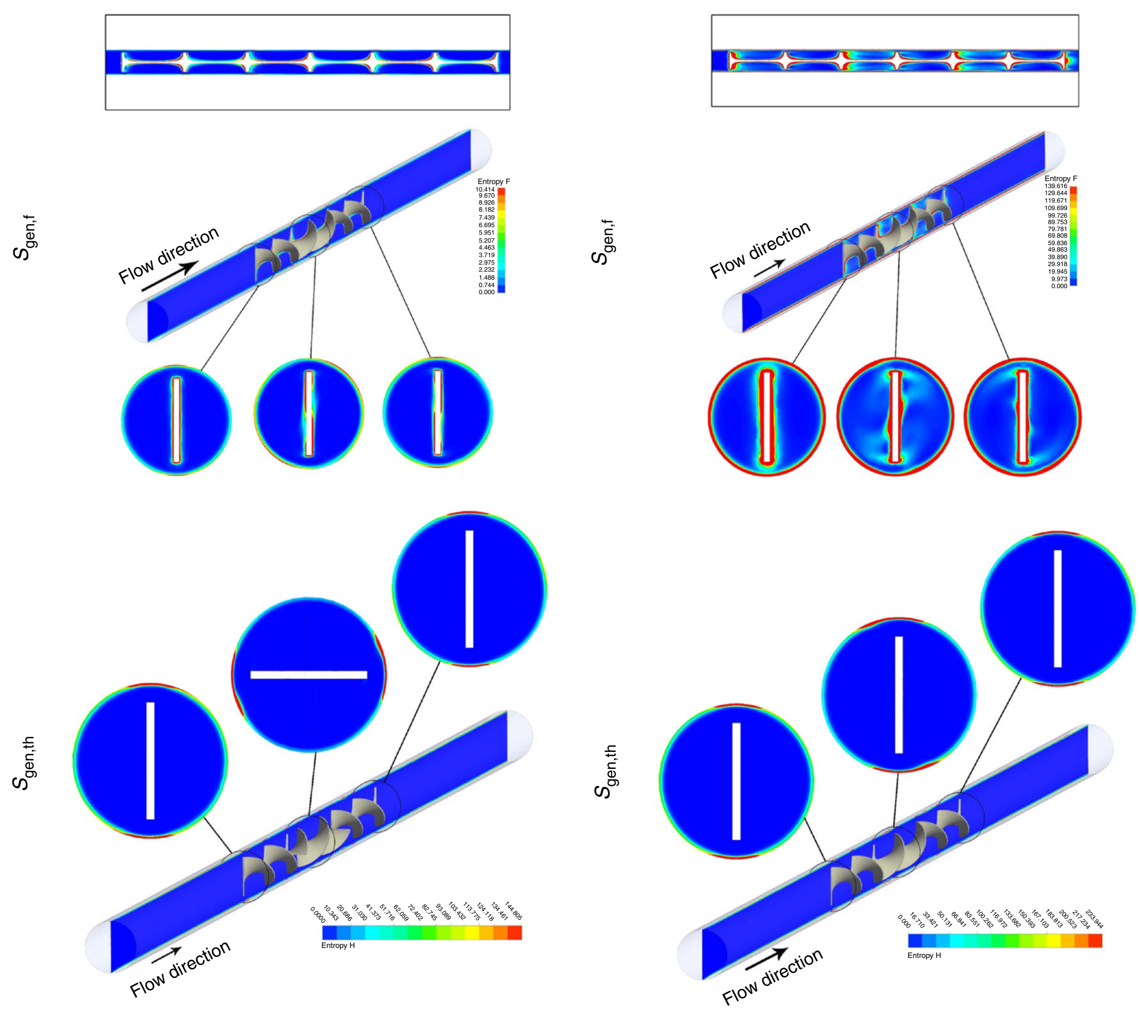

Fig. 3 Frictional and thermal entropy generation contours at $\beta = 0°$, $Re = 5000$

Results and discussion

Entropy generation of turbulent nanofluid flow within a duct with innovative swirling inserts was investigated in the current article. A homogenous model was considered.

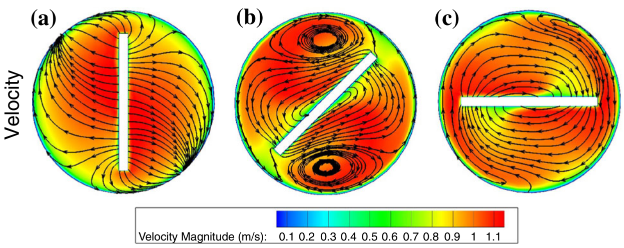

Fig. 4 Frictional, thermal entropy generation and velocity contours at $\beta = 0°, \quad Re = 20000$

We selected two parameters as variables (inlet velocity and revolution angle). Finding the best performance in view of thermal and second-law behaviors was our main purpose.

Impacts of inlet velocity and β on velocity contours, thermal and viscous entropy generation contours are depicted in Figs. 3–8. As inlet velocity enhances, pressure drop and temperature gradient increase. As inlet velocity increases, a reduction in the thermal boundary layer thickness can be observed, and it makes convective flow stronger. Pressure loss enhances due to a more swirling flow.

Secondary flow increases with augment of β, and in turn convective flow increases. Stronger turbulent intensity occurs for higher values of β. So, greater revolution angle makes to reach better nanofluid fluid mixing. The impact of β is more significant at lower inlet velocity because of thicker boundary layer in low Reynolds number. Also,

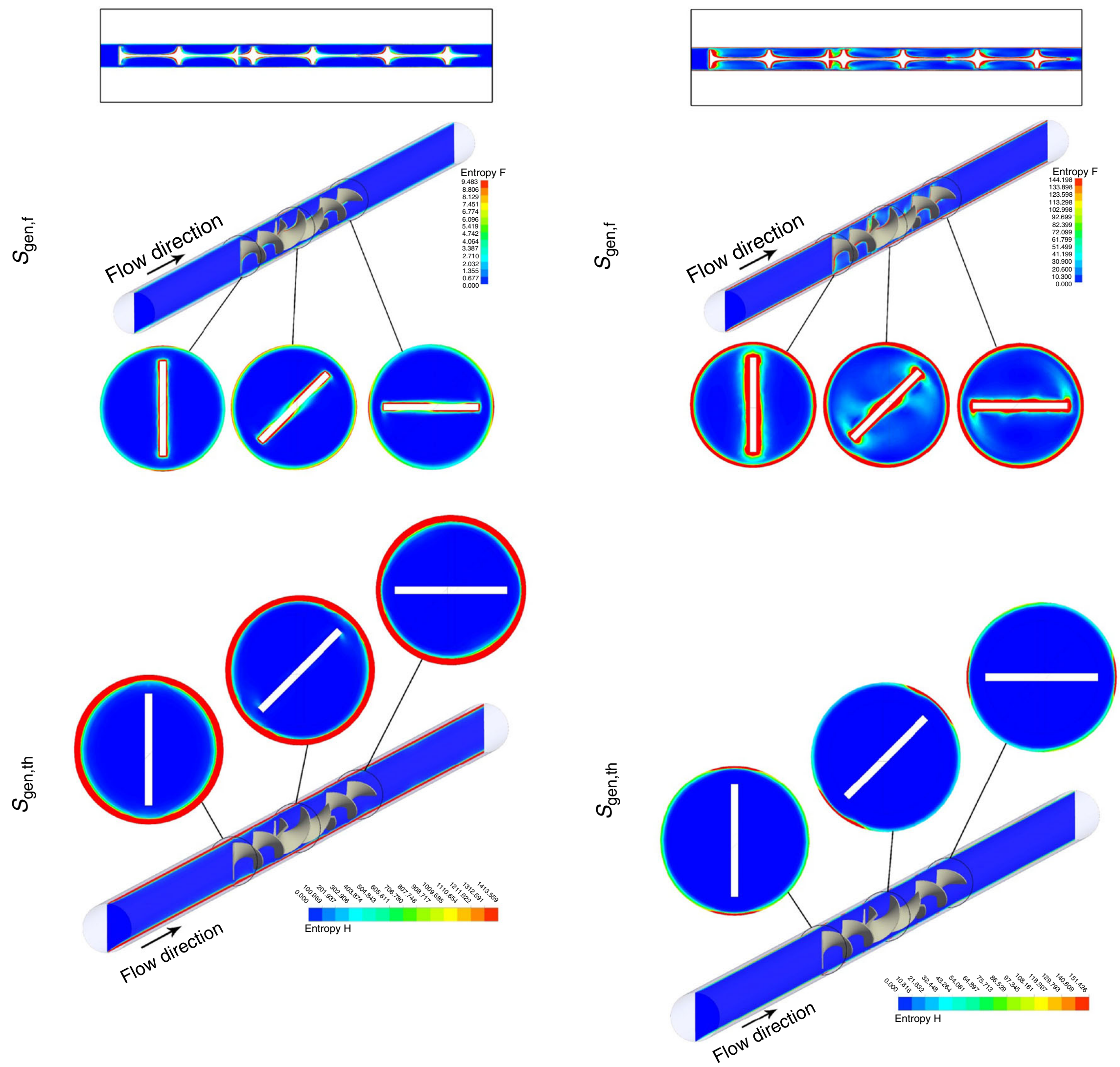

Fig. 5 Frictional and thermal entropy generation contours at $\beta = 45°, \quad Re = 5000$

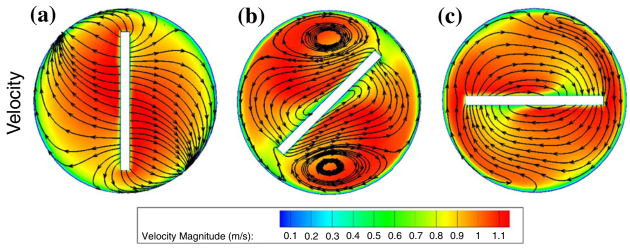

Fig. 6 Frictional, thermal entropy generation, and velocity contours at $\beta = 45°, \quad Re = 20000$

disruption of thermal boundary is more pronounced in lower Re. ΔP augments with an increase in β because of intensification in secondary flow.

Viscous entropy generation augments with augment of ΔP. So, $S_{\mathrm{gen,f}}$ intensifies with augment of inlet velocity and

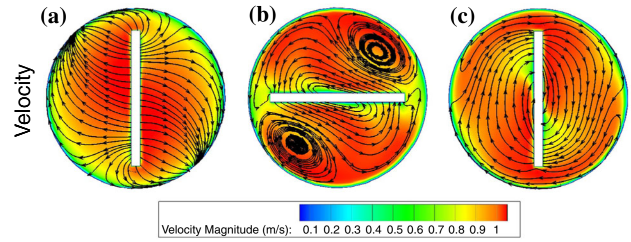

Fig. 8 Frictional, thermal entropy generation and velocity contours at $\beta = 90°, \quad Re = 20000$

revolution angle. Thermal entropy generate act against pressure loss. $S_{\mathrm{gen,th}}$ intensifies with a reduction in β and Re. The following formulas are derived for $S_{\mathrm{gen,th}}$, Be and $S_{\mathrm{gen,f}}$:

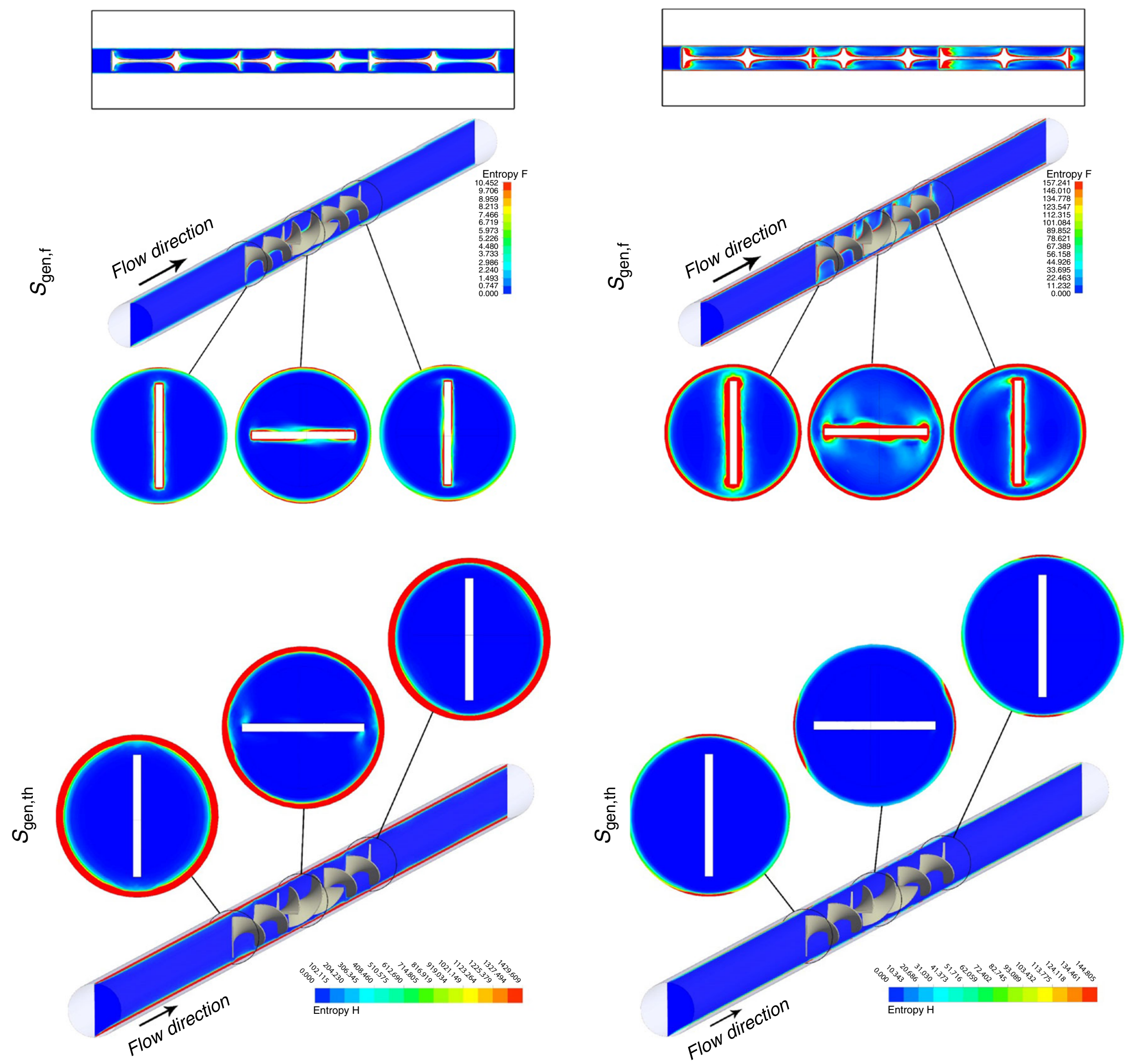

Fig. 7 Frictional and thermal entropy generation contours at $\beta = 90°, \quad Re = 5000$

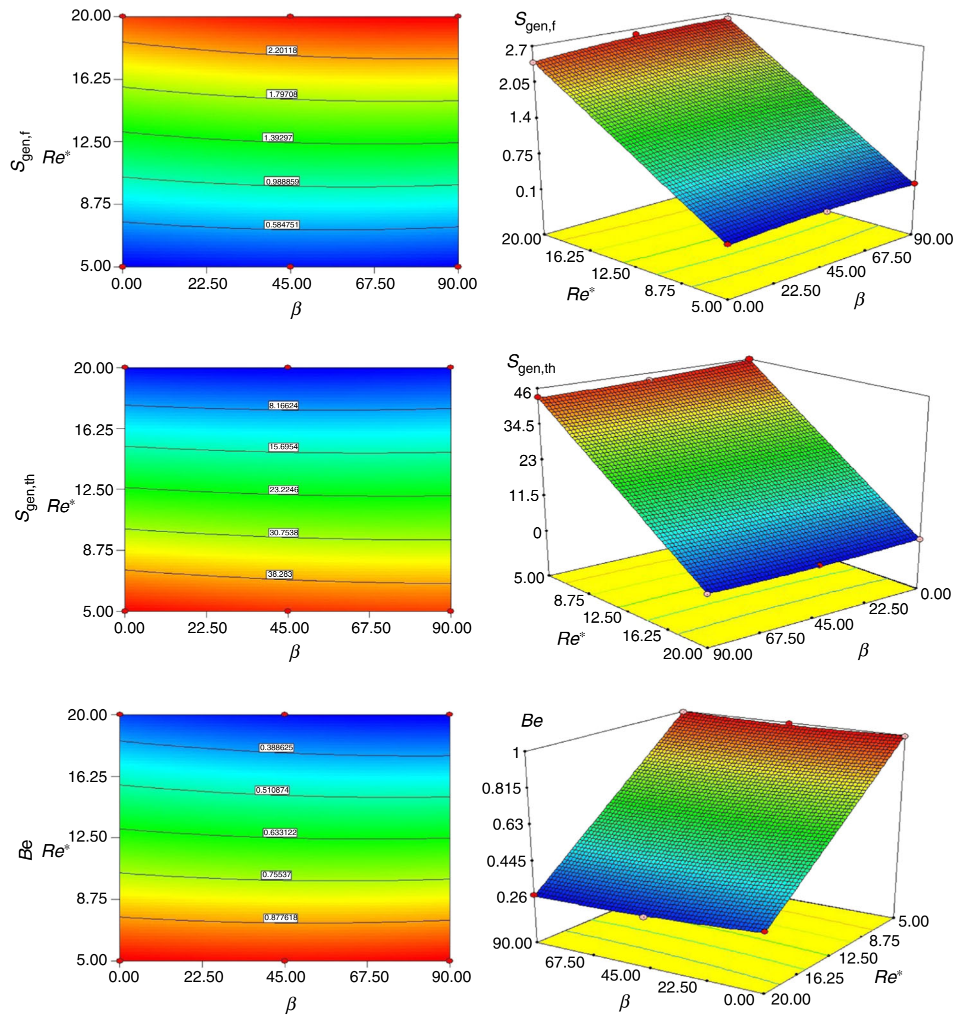

Fig. 9 Effects of Re and β on $S_{gen,f}, S_{gen,th}, Be$

$$S_{gen,th} = 22.26 - 0.73\beta - 21.62Re^{*} + 0.64\beta\, Re^{*} + 0.57\beta^{2} \tag{19}$$

$$Be = 0.63 - 0.012\beta - 0.35Re^{*} - 0.012\beta\, Re^{*} + 0.012\beta^{2} \tag{20}$$

$$S_{gen,f} = 1.4 + 0.049\beta + 1.16Re^{*} + 0.039\beta\, Re^{*} - 0.048\beta^{2} \tag{21}$$

In the above equations, $Re^{*} = 0.001Re$ and mean square error is 0.98. Figure 9 demonstrates the impacts of β and Re on entropy parameters. Secondary vortexes become stronger with an increase in both parameters. Therefore, $S_{gen,th}$ is an augmenting function of Re and β. Roles of significant parameters on $S_{gen,f}$ are different from $S_{gen,th}$. So, $S_{gen,th}$ reduces with augment of Re and β. Because of higher values of $S_{gen,th}$ in comparison with $S_{gen,f}$, it can be concluded that Be detracts with an increase in Re and β.

Conclusions

In the current article, we simulate nanofluid entropy generation and heat transfer to find the best design for the current heat exchanger. In industries, designers want to reach the highest heat transfer rate and the lowest entropy generation. So, we attempted to show not only the hydrothermal behavior but also frictional and thermal entropy generations. We demonstrated the contours for various cases and extracted new correlations for goal factors. To estimate characteristics of nanofluid, previous experimental formulas have been employed. Results demonstrated that Bejan number reduces with intensification of inlet velocity and revolution angle. Thermal entropy generation reduces with an increase in both variable factors.

Acknowledgements This article was supported by the National Sciences Foundation ofChina (NSFC) (No. U1610109), UOW Vice-

Chancellor's Postdoctoral Research Fellowship.Also, the authors acknowledge the funding support of Babol Noshirvani University ofTechnology through Grant program No. BNUT/390051/97.

References

1. Rashidi S, Mahian O, Mohseni Languri E. Applications of nanofluids in condensing and evaporating systems. J Therm Anal Calorim. 2018;131:2027–39.
2. Sheikholeslami M. Numerical simulation for solidification in a LHTESS by means of Nano-enhanced PCM. J Taiwan Inst Chem Eng. 2018;86:25–41.
3. Sheikholeslami M. Solidification of NEPCM under the effect of magnetic field in a porous thermal energy storage enclosure using CuO nanoparticles. J Mol Liq. 2018;263:303–15.
4. Sheikholeslami M, Darzi M, Li Z. Experimental investigation for entropy generation and exergy loss of nano-refrigerant condensation process. Int J Heat Mass Transf. 2018;125:1087–95.
5. Jafaryar M, Sheikholeslami M, Li Z, Moradi R. Nanofluid turbulent flow in a pipe under the effect of twisted tape with alternate axis. J Therm Anal Calorim. 2018. https://doi.org/10.1007/s10973-018-7093-2.
6. Jafaryar M, Sheikholeslami M, Li Z. CuO–water nanofluid flow and heat transfer in a heat exchanger tube with twisted tape turbulator. Powder Technol. 2018;336:131–43.
7. Haq RU, Hommouch Z, Hussain ST, Mekkaoui T. MHD mixed convection flow along a vertically heated sheet. J Hydrogen Energy. 2017;42(24):15925–32.
8. Qi C, Liu M, Wang G, Pan Y, Liang L. Experimental research on stabilities, thermophysical properties and heat transfer enhancement of nanofluids in heat exchanger systems. Chin J Chem Eng. 2018. https://doi.org/10.1016/j.cjche.2018.03.021.
9. Sheikholeslami M, Jafaryar M, Saleem S, Li Z, Shafee A, Jiang Y. Nanofluid heat transfer augmentation and exergy loss inside a pipe equipped with innovative turbulators. Int J Heat Mass Transf. 2018;126:156–63.
10. Zheng N, Liu P, Liu Z, Liu W. Numerical simulation and sensitivity analysis of heat transfer enhancement in a flat heat exchanger tube with discrete inclined ribs. Int J Heat Mass Transf. 2017;112:509–20.
11. Sajjadi H, Kefayati GHR. MHD turbulent and laminar natural convection in a square cavity utilizing lattice Boltzmann method. Heat Transfer Asian Research. 2016;45(8):795–814.
12. Zheng N, Liu P, Shan F, Liu J, Liu Z, Liu W. Numerical studies on thermo-hydraulic characteristics of laminar flow in a heat exchanger tube fitted with vortex rods. Int J Therm Sci. 2016;100:448–56.
13. Astanina MS, Sheremet MA, Oztop HF, Abu-Hamdeh N. MHD natural convection and entropy generation of ferrofluid in an open trapezoidal cavity partially filled with a porous medium. Int J Mech Sci. 2018;136:493–502.
14. Mahian O, Oztop HF, Pop I, Mahmud S, Wongwises S. Design of a vertical annulus with MHD flow using entropy generation analysis. Thermal Science. 2013;17(4):1013–22.
15. Maleki H, Safaei, Alrashed AAA, Kasaeian A. Flow and heat transfer in non-Newtonian nanofluids over porous surfaces. J Therm Anal Calorim. 2018. https://doi.org/10.1007/s10973-018-7277-9.
16. Khan M, Irfan M, Khan WA, Ahmad L. Modeling and simulation for 3D magneto Eyring-Powell nanomaterial subject to nonlinear thermal radiation and convective heating. Results Phys. 2017;7:1899–906.
17. Sheikholeslami M, Jafaryar M, Li Z. Second law analysis for nanofluid turbulent flow inside a circular duct in presence of twisted tape turbulators. J Mol Liq. 2018;263:489–500.
18. Mahian O, Kianifar A, Sahin AZ, Wongwises S. Heat transfer, pressure drop, and entropy generation in a solar collector using SiO2/water nanofluids: effects of nanoparticle size and pH. J Heat Transfer. 2015;137:061011.
19. Goodarzi M, Kherbeet ASh, Afrand M, Sadeghinezhad E. Investigation of heat transfer performance and friction factor of a counter-flow double-pipe heat exchanger using nitrogen-doped, graphene-based nanofluids. Int Commun Heat Mass Transfer. 2016;76:16–23.
20. Nasiri H, Yaghoub M, Jamalabadi A, Sadeghi R, Safaei MR. Truong Khang Nguyen, Mostafa Safdari Shadloo, A smoothed particle hydrodynamics approach for numerical simulation of nanofluid flows: application to forced convection heat transfer over a horizontal cylinder. J Thermal Analysis Calorimetry, 2018, Accepted for publication.
21. Sheikholeslami M. Finite element method for PCM solidification in existence of CuO nanoparticles. J Mol Liq. 2018;265:347–55.
22. Sheikholeslami M, Ghasemi A, Li Z, Shafee A, Saleem S. Influence of CuO nanoparticles on heat transfer behavior of PCM in solidification process considering radiative source term. Int J Heat Mass Transf. 2018;126:1252–64.
23. Sheikholeslami M, Shehzad SA, Li Z, Shafee A. Numerical modeling for Alumina nanofluid magnetohydrodynamic convective heat transfer in a permeable medium using Darcy law. Int J Heat Mass Transf. 2018;127:614–22.
24. Ramzan M, Chung JD, Ullah N. Partial slip effect in the flow of MHD micropolar nanofluid flow due to a rotating disk—a numerical approach. Results Phys. 2017;7:3557–66.
25. Andrzejczyk R, Muszynski T. An experimental investigation on the effect of new continuous core-baffle geometry on the mixed convection heat transfer in shell and coil heat exchanger. Appl Therm Eng. 2018;136:237–51.
26. Sheikholeslami M, Jafaryar M, Shafee A, Li Z. Investigation of second law and hydrothermal behavior of nanofluid through a tube using passive methods. J Mol Liq. 2018;269:407–16.
27. Sheikholeslami M, Li Z, Shafee A. Lorentz forces effect on NEPCM heat transfer during solidification in a porous energy storage system. Int J Heat Mass Transf. 2018;127:665–74.
28. Sheikholeslami M. New computational approach for exergy and entropy analysis of nanofluid under the impact of Lorentz force through a porous media. Comp Meth Appl Mech Eng. (forthcoming). https://doi.org/10.1016/j.cma.2018.09.044.
29. Sheikholeslami M. Numerical approach for MHD Al2O3-water nanofluid transportation inside a permeable medium using innovative computer method. Comp Meth Appl Mech Eng. (forthcoming). https://doi.org/10.1016/j.cma.2018.09.042.
30. Sheikholeslami M. Application of Darcy law for nanofluid flow in a porous cavity under the impact of Lorentz forces. J Mol Liq. 2018;266:495–503.
31. Ali F, Ahmad Sheikh N, Khan I, Saqib M. Magnetic field effect on blood flow of Casson fluid in axisymmetric cylindrical tube: a fractional model. J Magn Magn Mater. 2017;423:327–36.
32. Estellé P, Mahian O, Maré T, Öztop HF. Natural convection of CNT water-based nanofluids in a differentially heated square cavity. J Therm Anal Calorim. 2017;128:1765–70.
33. Khan NS, Gul T, Islam S, Kha A, Shah Z. Brownian motion and thermophoresis effects on MHD mixed convective thin film second-grade nanofluid flow with hall effect and heat transfer past a stretching sheet. J Nanofluids. 2017;6:1–18.
34. Sheikholeslami M. Influence of magnetic field on Al2O3-H2O nanofluid forced convection heat transfer in a porous lid driven cavity with hot sphere obstacle by means of LBM. J Mol Liq. 2018;263:472–88.

35. Esfe MH, Saedodin S, Mahian O, Wongwises S. Thermal conductivity of Al2O3/water nanofluids. J Therm Anal Calorim. 2016;117(2):675–81.
36. Sheikholeslami M, Shehzad SA, Li Z. Water based nanofluid free convection heat transfer in a three dimensional porous cavity with hot sphere obstacle in existence of Lorenz forces. Int J Heat Mass Transf. 2018;125:375–86.
37. Maskaniyan M, Nazari M, Rashidi S, Mahian O. Natural convection and entropy generation analysis inside a channel with a porous plate mounted as a cooling system. Thermal Sci Eng Progress. 2018;6:186–93.
38. Sheikholeslami M, Jafaryar M, Li Z. Nanofluid turbulent convective flow in a circular duct with helical turbulators considering CuO nanoparticles. Int J Heat Mass Transf. 2018;124:980–9.
39. Fengrui S, Yuedong Y, Xiangfang L. The heat and mass transfer characteristics of superheated steam coupled with non-condensing gases in horizontal wells with multi-point injection technique. Energy. 2018;143:995–1005.
40. Sheikholeslami M. Investigation of Coulomb forces effects on Ethylene glycol based nanofluid laminar flow in a porous enclosure. Appl Math Mech (English Edition). 2018;39(9):1341–52.
41. Sheikholeslami M, Rokni HB. Simulation of nanofluid heat transfer in presence of magnetic field: A review. Int J Heat Mass Transf. 2017;115:1203–33.
42. Akar S, Rashidi S, Abolfazli Esfahani J. Second law of thermodynamic analysis for nanofluid turbulent flow around a rotating cylinder. J Therm Anal Calorim. 2017. https://doi.org/10.1007/s10973-017-6907-y.
43. Al-Rashed AAAA, Aich W, Kolsi L, Mahian O, Hussein AK, Borjini MN. Effects of movable-baffle on heat transfer and entropy generation in a cavity saturated by CNT suspensions: three-dimensional modeling. Entropy. 2017;19(5):200.
44. Koo J, Kleinstreuer C. Viscous dissipation effects in micro tubes and micro channels. Int J Heat Mass Transf. 2004;47:3159–69.
45. Kim D, Kwon Y, Cho Y, Li C, Cheong S, Hwang Y, Lee J, Hong D, Moona S. Convective heat transfer characteristics of nanofluids under laminar and turbulent flow conditions. Curr Appl Phys. 2009;9:119–23.